

Streamer Formation in Plasma with a Temperature Gradient

J. F. Drake, P. N. Guzdar, and A. B. Hassam

Laboratory for Plasma Research, University of Maryland, College Park, Maryland 20742

(Received 18 April 1988)

Turbulence produced by a temperature gradient in a collisional plasma is investigated. The system evolves to a state in which highly elongated streams of plasma move up and down the temperature gradient. The resulting transport greatly exceeds estimates based on mixing-length arguments. It is argued that such streams are the preferred nonlinear state of turbulent fluctuations driven by both ∇T_e and ∇T_i .

PACS numbers: 52.25.Fi, 52.35.Qz

A plasma with a sufficiently large electron or ion temperature gradient develops a negative compressibility and consequently becomes unstable. There is increasing evidence that the resulting η_e (driven by ∇T_e) and η_i (driven by ∇T_i) instabilities¹⁻⁴ may be a cause of the anomalous transport in tokamaks. While the linear stability of these modes⁵⁻⁷ is now fairly well understood, the nonlinear saturation of the fluctuations and associated thermal transport are still under investigation.

In the present Letter we focus on the nonlinear behavior of a very simple straight magnetic field configuration with an electron temperature gradient. A set of nonlinear equations describing the η_e mode is derived from the Braginskii fluid equations and solved numerically. The calculation is specifically carried out for the η_e instability; however, we believe that the formation of streamers is generic to both the η_e and η_i modes. The turbulent fluctuations exhibit a spontaneous transition to a state of enhanced transport in which highly elongated vortices (streamers) enable the fluid to take large steps along the temperature gradient. In a simple analytic calculation we demonstrate that these streamers are the preferred nonlinear state of the system. An analogous analytic calculation applies equally well to the η_i instability. Thus, the formation of streamers is apparently generic to these ∇T -driven, negative-compressibility modes. In this novel regime the thermal transport D_\perp greatly exceeds that given from the simple expression $D_\perp \sim \gamma/k_\perp^2$ which is widely invoked in the literature.

In the η_e instability the electrons behave like a fluid while the ions, because $k_\perp \rho_i > 1$, respond adiabatically, $\tilde{n}/n \approx -e\tilde{\phi}/T_i$, where \tilde{n} and $\tilde{\phi}$ are the density and potential perturbations.⁵ In the fluid limit $\partial/\partial t \ll \nu_{ei}$, the local linear growth of the basic instability is given by $\gamma_\eta = 1.71 k_\parallel^2 D_{\parallel e} (\eta_e - 1)$, where $D_{\parallel e}$ is the parallel electron diffusion coefficient, k_\parallel is the parallel wave vector, and $\eta_e = d \ln T_e / d \ln n$.⁸ The unstable domain of the mode in k space is limited by classical perpendicular transport $D_{\perp e}$ at short scales ($\gamma_\eta > k_\perp^2 D_{\perp e}$) and by electromagnetic effects at long scales ($k_\perp^2 D_r > \gamma_\eta$, with $D_r = \eta_i c^2 / 4\pi$ the classical flux diffusion rate). The diamagnetic propagation stabilizes short parallel wavelengths [$\gamma_\eta < \omega_* = k_y V_{*n}$, with $V_n = cT_e / eBL_n$ and

$$L_n = (d \ln n / dx)^{-1}].$$

A set of nonlinear equations describing the instability in a uniform magnetic field B_0 can be derived from the reduced Braginskii fluid equations.⁹ In dimensionless form they are the continuity, electron temperature, and flux diffusion equations,

$$dn/dt - \beta \nabla_\perp^2 n = -\beta \nabla_\perp^2 T/4 - \mathbf{b} \cdot \nabla \nabla_\perp^2 \psi, \quad (1)$$

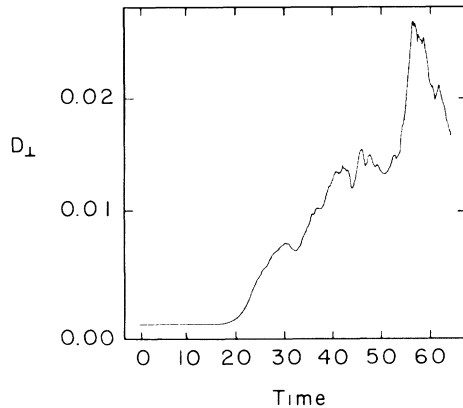
$$\begin{aligned} \frac{3}{2} dT/dt - 1.6(\mathbf{b} \cdot \nabla)^2 T - 1.35\beta \nabla_\perp^2 T \\ = -(\beta/2)\nabla_\perp^2 n - 1.71\mathbf{b} \cdot \nabla \nabla_\perp^2 \psi, \end{aligned} \quad (2)$$

$$\partial\psi/\partial t - \nabla_\perp^2 \psi = \mathbf{b} \cdot \nabla n + 1.71\mathbf{b} \cdot \nabla T - \mathbf{b} \cdot \nabla \phi, \quad (3)$$

with $d/dt = \partial/\partial t + \mathbf{v}_\perp \cdot \nabla$, $\mathbf{v}_\perp = -\nabla\phi \times \hat{z}$, and $\mathbf{b} \cdot \nabla = \partial/\partial z + \nabla\psi \times \hat{z} \cdot \nabla$. The dimensionless variables are defined by $TL_n/L_\perp T_0 \rightarrow T$, $nL_n/L_\perp n_0 \rightarrow n$, $\psi L_\parallel / B_0 L_\perp^2 \rightarrow \psi$, $x/L_\perp \rightarrow x$, $y/L_\perp \rightarrow y$, $z/L_\parallel \rightarrow z$, and $t/\tau \rightarrow t$, with the perpendicular and parallel scale lengths given by $L_\perp = D_r/V_{*n}$ and $L_\parallel = (D_{\parallel e} D_r)^{1/2}/V_{*n}$ and the time scale by $\tau = D_r/V_{*n}^2$. In Eqs. (1)-(3) the terms proportional to β result from cross-field, classical transport, the term proportional to $(\mathbf{b} \cdot \nabla)^2$ in Eq. (2) arises from parallel thermal conduction, and the last terms on the right-hand side of Eqs. (1) and (2) arise from parallel electron compression. In a plasma with an initially uniform density and temperature gradient, $T = \tilde{T} + \eta_e x$, $n = \tilde{n} + x$, and $\phi = -\tilde{n}$.

In the dimensionless equations the characteristic transport rate is $D_\perp \sim L_\perp^2/\tau \sim D_r$, the flux diffusion rate. This result is a consequence of our choice for L_\perp which corresponds to the long-wavelength, electromagnetic cutoff of the unstable spectrum. A choice for L_\perp based on the short-wavelength cutoff of the spectrum results in the characteristic diffusion rate $D_\perp \sim D_{\perp e} \sim \beta D_r$, the classical transport rate. Most generally, we must have $D_\perp = D_r f(\beta, \eta_e)$ since β and η_e are the only independent parameters of Eqs. (1)-(3). The sensitivity of f to β will determine whether long or short wavelengths dominate the transport.

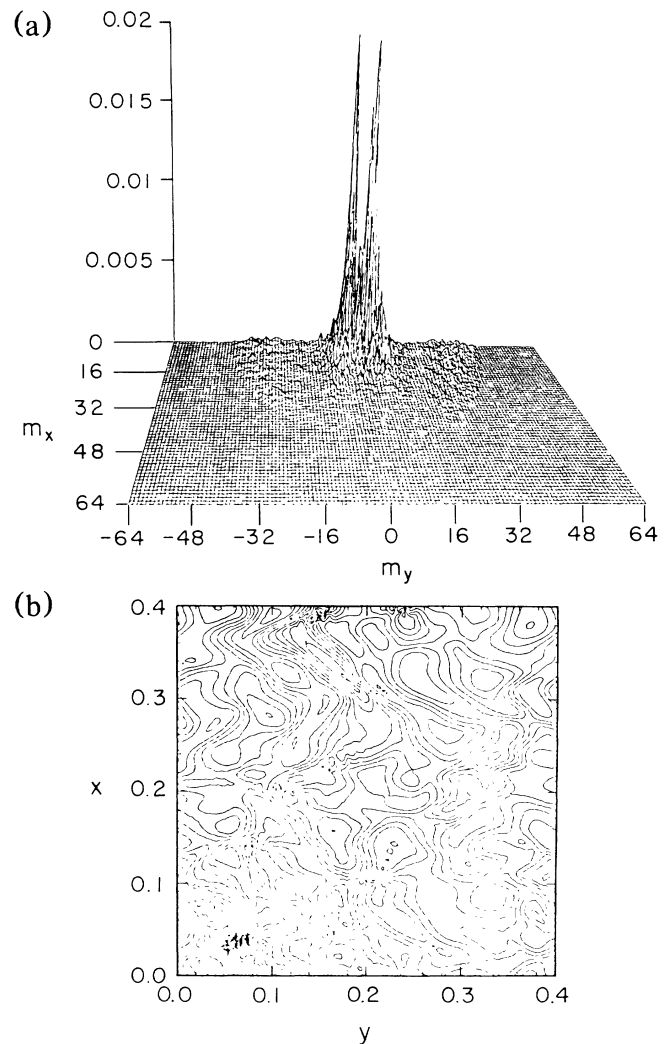
Equations (1)-(3) have been reduced to 2D by our assuming that n , T , ϕ , and ψ in Eqs. (1)-(3) are functions only of x and $y+az$, with a a constant so that $\partial/\partial z = a \partial/\partial y$. The equations are then integrated from

FIG. 1. Anomalous transport D_{\perp}/D_r vs time.

random initial conditions with a pseudospectral code.¹⁰ Insensitivity of the results to time step and grid spacing has been carefully verified. A large number of runs have been completed on grids ranging from 32×32 to 128×128 , most having been run on the finer grid.

In Fig. 1 we plot the anomalous transport coefficient D_{\perp} versus time for a 128×128 run with $\eta_e = 3.5$, $\beta = 0.001$, and $\alpha = 0.35$. The transport rate saturates around $t = 28$ and then rises to a much higher level at late time. In Fig. 2 we show plots of $|\tilde{\phi}_k| = -|\tilde{n}_k|$ in k space [$\mathbf{m} = (0.4k_x, 2.0k_y)$] and contours of $\tilde{\phi}(x, y)$ in configuration space at $t = 32$, where D_{\perp} first saturates. The two large peaks in Fig. 2(a) fall in the region of linear instability. The linear growth rate is symmetric around $m_y = 0$ and the most unstable mode is given by $\mathbf{m} = (4, \pm 6)$. The linearly unstable region of the spectrum occupies only a very small region of the grid. Computationally we require a very large number of linearly stable modes at large $|\mathbf{k}|$ in order for the results to be insensitive to the grid boundaries. The physical reason for this requirement will be explicated shortly. The constant potential contours in Fig. 2(b) are the streamlines of the fluid flow. They form closed vortices.

In Fig. 3 we show plots of $|\tilde{\phi}_k|$ and contours of $\tilde{\phi}(x, y)$ and $T(x, y)$ at late time when $D_{\perp} \approx 0.06$ is much greater than in Fig. 2. The spectrum of $|\tilde{\phi}_k|$ in Fig. 3(a) has several noteworthy features: The spectrum has become strongly asymmetric around $k_y = 0$; the spectrum has become extremely peaked around $\mathbf{m} = (2, -3)$ (the longest-wavelength unstable mode in the grid); and low-level fluctuations extend all the way to the boundary. The potential contours corresponding to this asymmetric spectrum in Fig. 3(b) are extremely elongated in comparison with those in Fig. 2(b), enabling the high-temperature plasma to stream down the gradient and the low-temperature plasma to stream up the gradient with a very large step size. As a consequence, a very steep gradient in the local temperature forms at the boundary between the opposing flows which can be seen in the contour plot of $T(x, y)$ in Fig. 3(c). This local gradient destabilizes very-short-wavelength modes which appear

FIG. 2. (a) Plot of $|\tilde{\phi}_k|$ in k space [$\mathbf{m} = (0.4k_x, 2.0k_y)$] and (b) corresponding contours of $\tilde{\phi}(x, y)$ in configuration space at $t = 32$.

along the elongated vortex in Fig. 3(b) and in the spectral plot in Fig. 3(a). The transport resulting from these elongated vortices is of order $D_{\perp} \sim 0.06D_r$, compared with the traditional estimate $D_{\perp} = \gamma/k_{\perp}^2 \sim 0.006D_r$ for the $\mathbf{m} = (2, -3)$ mode. The formation of this strongly asymmetric spectrum has been observed in all of our simulations. The spectrum can peak at k_y positive or negative, depending on the initial conditions. In some cases the peak of the spectrum has been observed to flip from $k_y < 0$ to $k_y > 0$ or vice versa. During the transition the transport is greatly reduced so that D_{\perp} does not simply approach a constant at late time. It changes erratically.

We now present a simple calculation which demonstrates that the asymmetric state is favored over the symmetric state. We retain only the essential terms in Eqs. (1) to (3) which describe the linear stability and the dominant nonlinearities. In the electrostatic limit, Eq.

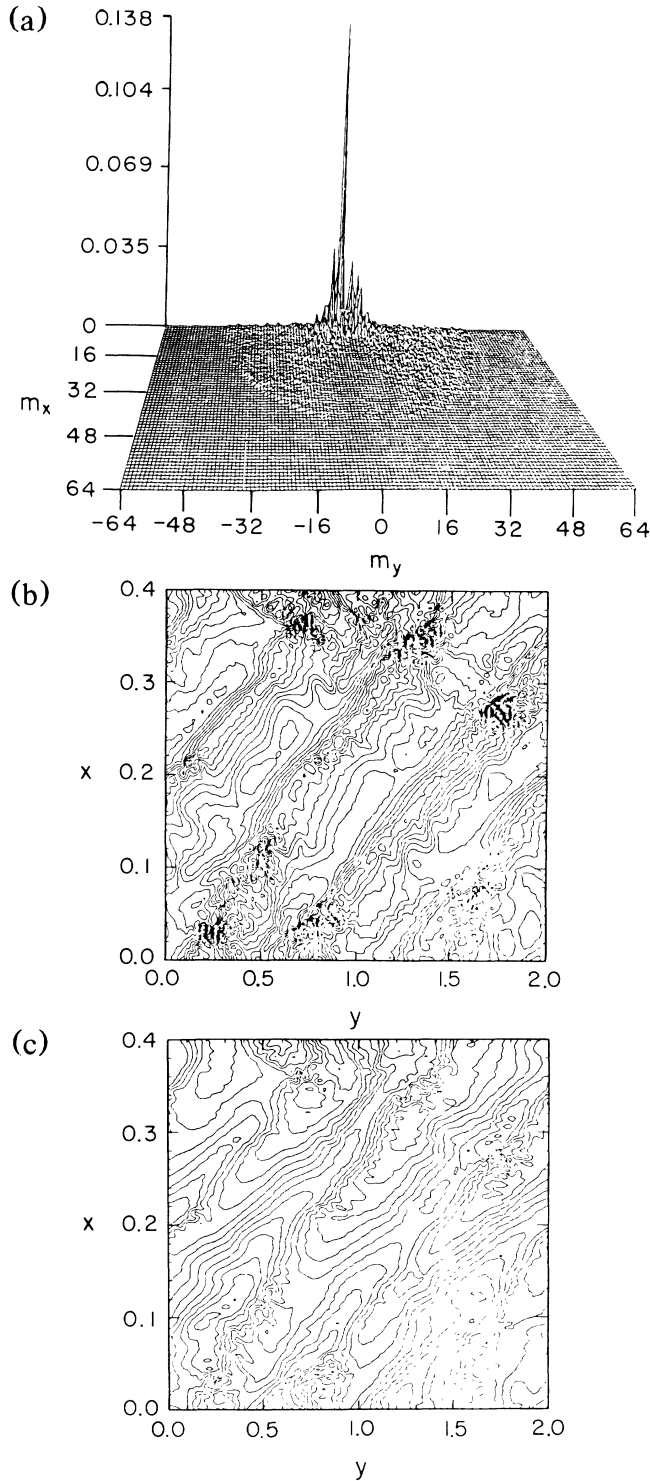


FIG. 3. (a) Plot of $|\tilde{\phi}_k|$ in k space and (b) corresponding contours of $\tilde{\phi}(x,y)$ and (c) $T(x,y)$ at late time.

(3) reduces to $\nabla_{\perp}^2 \psi = -1.71\alpha \tilde{T}_y$ and Eqs. (1) and (2) become

$$\partial \tilde{n} / \partial y = +1.71\alpha^2 \partial^2 \tilde{T} / \partial y^2, \quad (4)$$

$$\partial \tilde{T} / \partial t - 0.9\beta \nabla_{\perp}^2 \tilde{T} + \nabla \tilde{n} \times \tilde{z} \cdot \nabla \tilde{T} = -\eta_e \partial \tilde{n} / \partial y. \quad (5)$$

The convection of the temperature in Eq. (5) is the dominant nonlinearity in the electrostatic limit. The simplest model which reproduces the breaking of the symmetry observed in the simulations is the interaction of the three waves,

$$\tilde{T} = T_+ \cos(px + qy) + T_- \cos(px - qy) + T_0 \sin(2px), \quad (6)$$

with \tilde{n} given by Eq. (4). Inserting Eq. (6) into Eq. (5), we obtain a set of coupled nonlinear equations for T_+ , T_- , and T_0 ,

$$\dot{T}_{\pm} - \gamma_{\eta} T_{\pm} - MT_0 T_{\mp} = 0, \quad (7)$$

$$\dot{T}_0 + \gamma_{\beta} T_0 + 2MT_+ T_- = 0, \quad (8)$$

with $\gamma_{\eta} = 1.71\alpha^2 q^2 \eta_e$, the linear growth rate of the instability, $\gamma_{\beta} = 0.9\beta(p^2 + q^2)$, the damping from classical cross-field transport, and $M = 1.71\alpha^2 pq^2$. These equations yield the equilibrium solution

$$T_0 = -\gamma_{\eta}/M; \quad T_{\pm}^2 = \gamma_{\beta} \gamma_{\eta} / 2M^2; \quad T_- = T_+. \quad (9)$$

Physically this solution corresponds to periodic vortex rolls [$\tilde{T} \sim T_+ \cos(px) \cos(qy)$] which quasilinearly flatten the local temperature gradient [$\partial \tilde{T} / \partial x \sim 2\eta_e \times \cos(2px)$]. This state is similar to that shown in Fig. 2 and results in the rather low level of transport at $t \approx 30$ in Fig. 1. Linearizing Eqs. (8) and (9) around this solution, we find that it is unstable with a growth rate $\gamma = 2\gamma_{\eta}$, and eigenfunctions $\tilde{T}_+ = -\tilde{T}_-$ with $\tilde{T}_0 = 0$. Thus, either T_+ or T_- increases and its counterpart decreases, as is seen in the simulations. The large-time solutions in Eqs. (7) and (8) always correspond to either T_+ or T_- growing exponentially ($\gamma = \gamma_{\eta}$) and completely dominating the remaining two modes. In this case the flow pattern corresponds to plane sheets at a finite angle with respect to the direction of the original gradient. More modes must be included to saturate the instability and form the elongated vortices seen in the simulation. It is the formation of these vortices which allows the transport to rise dramatically for $t > 32$ in Fig. 1.

A number of runs have been completed with different values of β and η_e to determine the scaling of D_{\perp} (maximum value) with these parameters. We assume that the transport can be modeled by the simple function

$$D_{\perp} / D_r = a\beta^{\epsilon} (\eta_e - \eta_{ec})^{\delta}, \quad (10)$$

where η_{ec} is the critical value of η_e required for instability. Unfortunately, η_{ec} depends weakly on β . The values $\epsilon = 0$, $\delta = 2.5$, and $a = 0.025$ fit the data very well. Thus, we conclude that the long-wavelength modes dominate the transport, which is not too surprising considering the peakedness of the spectrum in this region and the nature of the flow pattern in Fig. 3(b). The scaling of D_{\perp} with η_e in Eq. (10) is valid only for $\eta_e - \eta_{ec}$ not too large. For very large η_e , we can rescale Eqs. (1)-(3), eliminate η_e as a parameter, and show that the transport again

scales as D_r , independent of η_e . Finally, numerical computations have also been completed for $\alpha=0.28$. The ϕ and T fluctuations are qualitatively the same as those shown in Figs. 1-3 (the fluctuations extended to somewhat larger wavelengths) but D_\perp was essentially unchanged. The insensitivity of the results to α provide some confidence that a full 3D simulation will produce similar results.

We have shown that fluctuations driven by η_e form highly elongated vortices or streamers which greatly enhance the transport over that which would be predicted from $D_\perp \sim \gamma/k_\perp^2$. Effectively, the system collapses to a quasi-one-dimensional state. Two interesting questions are the following: How general are these results in terms of applicability to other instabilities; and what will be the influence of magnetic shear on the streamers? Similar 2D calculations¹¹ of the nonlinear saturation of the η_i instability have recently been completed. Streamers again dominate the nonlinear behavior of the system. Streamers are also visible in recent simulations of the large-Larmor-radius interchange mode.¹² Magnetic shear only weakly affects the linear η_e and η_i instabilities. However, the significant elongation of the streamers along ∇T may be disrupted by magnetic shear and will be investigated in the future. Care must therefore be exercised in applying the present results directly to the tokamak confinement problem. On the other hand, our results have important implications for heating configurations with weak or no magnetic shear, such as some stellarators (Wendelstein VIIA), the central cell of tandem mirrors, and the central flat q region in tokamaks. Once a threshold in η_i or η_e is exceeded during heating, streamers will form in both the ion and electron temperature profiles, strongly degrading

confinement. Fortunately, this behavior can be mitigated by peaking the density profile as the plasma is heated so as to maintain $\eta_{e,i}$ below threshold across the entire profile. The development of techniques to control both density and temperature profiles is therefore essential to achieve efficient heating.

This work was supported in part by the U.S. Department of Energy.

¹P. N. Guzdar, C. S. Liu, J. Q. Dong, and Y. C. Lee, Phys. Rev. Lett. **57**, 2818 (1986).

²G. S. Lee and P. H. Diamond, Phys. Fluids (to be published).

³D. L. Brower *et al.*, Phys. Rev. Lett. **59**, 48 (1987).

⁴F. X. Soldner *et al.*, Phys. Rev. Lett. **61**, 1105 (1988).

⁵Y. C. Lee, J. Q. Dong, P. N. Guzdar, and C. S. Liu, Phys. Fluids **30**, 1331 (1987).

⁶B. B. Kadomtsev, in *Reviews of Plasma Physics*, edited by M. A. Leontovich (Consultants Bureau, New York, 1970), Vol. 5, p. 309.

⁷B. Coppi, M. N. Rosenbluth, and R. Z. Sagdeev, Phys. Fluids **10**, 582 (1967).

⁸V. A. Rozhanskii, Pis'ma Zh. Eksp. Teor. Fiz. **34**, 60 (1981) [JETP Lett. **34**, 56 (1981)].

⁹J. F. Drake and T. M. Antonsen, Phys. Fluids **27**, 898 (1984).

¹⁰D. Fyfe and D. Montgomery, Phys. Fluids **22**, 246 (1974).

¹¹J. F. Drake, A. B. Hassam, A. Dimits, and P. N. Guzdar, in Proceedings of the Joint Varenna-Lausanne International Workshop on Theory of Fusion Plasmas, 3-7 October 1988 (to be published).

¹²J. D. Huba, J. G. Lyon, and A. B. Hassam, Phys. Rev. Lett. **59**, 2971 (1987).